Journal of Magnetic Resonance 201 (2009) 165–174

Contents lists available at ScienceDirect

Journal of Magnetic Resonance

journal homepage: www.elsevier.com/locate/jmr

Directly and indirectly detected through-bond heteronuclear correlation solid-state NMR spectroscopy under fast MAS

Kanmi Mao, Marek Pruski *

Ames Laboratory, Iowa State University, Ames, IA 50011-3020, USA
Department of Chemistry, Iowa State University, Ames, IA 50011-3020, USA

ARTICLE INFO

Article history:
Received 9 July 2009
Available online 10 September 2009

Keywords:
Solid-state NMR
J-coupling
Fast MAS
HETCOR
INEPT
PMLG
Indirect detection
Peptide
Coal

ABSTRACT

Two-dimensional through-bond $^{1}H\{^{13}C\}$ solid-state NMR experiments utilizing fast magic angle spinning (MAS) and homonuclear multipulse ^{1}H decoupling are presented. Remarkable efficiency of polarization transfer can be achieved at MAS rates exceeding 40 kHz, which is instrumental in these measurements. Schemes utilizing direct and indirect detection of heteronuclei are compared in terms of resolution and sensitivity. A simple procedure for optimization of ^{1}H homonuclear decoupling sequences under these conditions is proposed. The capabilities of these techniques were confirmed on two naturally abundant solids, tripeptide *N-formyl*-L-methionyl-L-leucyl-L-phenylalanine (f-MLF-OH) and brown coal.

© 2009 Elsevier Inc. All rights reserved.

1. Introduction

Astounding advances are currently being made in solid-state NMR spectroscopy following the development of magic angle spinning (MAS) at rates approaching 70 kHz [1,2]. Recent reports have highlighted several advantages of fast MAS probes, including excellent sensitivity per spin and efficient cross-polarization (CP) transfer [3,4], the ability of generating very high radiofrequency (RF) magnetic fields, and the possibility of using low-power RF schemes during preparation, mixing and decoupling periods [5]. In addition, fast MAS affords increased frequency range of the indirect dimension in rotor-synchronized experiments and eliminates the spinning sidebands at high magnetic fields or in the presence of large chemical shifts anisotropies (CSAs). Most importantly, it helps to reduce or, in some cases, eliminate the strong homonuclear dipolar couplings between high-γ nuclei (^{1}H and ^{19}F). Indeed, fast MAS by itself enabled the acquisition of directly detected (also referred to as X-detected or $X\{^{1}H\}$) and indirectly detected (^{1}H-detected or $^{1}H\{X\}$) multi-dimensional heteronuclear correlation (HETCOR) NMR spectra of organic materials in which ^{1}H spin systems were isotopically diluted, exhibited some degree of motional narrowing, or were fully coupled [4,6–10]. In our studies, MAS at 40 kHz was used to achieve high ^{1}H resolution in mesoporous organic–inorganic hybrid materials [4]. The CRAMPS-quality resolution was attainable in such systems by MAS alone because the local molecular dynamics limited the ^{1}H linewidth to less than half of the static value. Subsequently, it became possible to enhance the sensitivity of through-space (i.e., using CP) two-dimensional (2D) HETCOR experiments by detecting the low-γ (X) nuclei indirectly via high-γ ^{1}H nuclei [8]. In the case of ^{1}H-detected HETCOR experiments, the sensitivity of indirect detection is typically several times better than that of the standard $X\{^{1}H\}$ method [6–10].

Most recently, it has been demonstrated that fast MAS is fully compatible with homonuclear ^{1}H decoupling using RF pulse sequences, either previously known yet deemed relevant only under MAS rates below 25 kHz, or newly designed [11,12]. Under optimal experimental conditions the resolution of ^{1}H spectra obtained under MAS at 40–70 kHz turned out to be comparable to or better than that obtained in previous state-of-the-art CRAMPS experiments [11]. Thus, fast MAS also offers new opportunities for through-bond heteronuclear spectroscopy, e.g. using pulse sequences similar to heteronuclear single quantum correlation (HSQC) experiments in solution NMR. The utility of using ^{1}H–^{1}H homonuclear decoupling during INEPT in ^{13}C-detected HETCOR experiments at a lower MAS rate (22 kHz) has been already demonstrated [13]. Indeed, decoupling using so-called "mind-boggling optimization" (DUMBO) during INEPT tripled the sensitivity in ^{13}C labelled L-isoleucine. The first ^{1}H-detected, INEPT based HETCOR spectra in weakly coupled spin systems have been reported, as well [14]. Fast MAS was instrumental in improving the efficiency of the

* Corresponding author. Address: Ames Laboratory, Iowa State University, 230 Spedding Hall, Ames, IA 50011-3020, USA. Fax: +1 515 294 4709.
E-mail address: mpruski@iastate.edu (M. Pruski).

1090-7807/$ - see front matter © 2009 Elsevier Inc. All rights reserved.
doi:10.1016/j.jmr.2009.09.004

INEPT transfer because it reduced the magnetization losses due to transverse relaxation.

Herein, we seek to maximize the efficiency of INEPT in HSQC-type experiments in fully rigid solids by combining ^{1}H–^{1}H RF decoupling with MAS at $\nu_R \geqslant 40$ kHz and investigate the sensitivity benefit of indirect detection. The choice of ^{1}H–^{1}H decoupling method during INEPT is not obvious, because the effectiveness of polarization transfer depends on the decoupling efficiency as well as the scaling factor. We provide a comprehensive analysis of the performance of several decoupling schemes (PMLG5$^{\bar{x}}_m$, PMLG5$^{\bar{x}\bar{x}}_{mm}$ and SAM3) during the INEPT transfer, and propose a simple optimization scheme for such experiments. The merit of the indirect approach (^{1}H{^{13}C}) is gauged against the results of a ^{13}C{^{1}H} HETCOR experiment in which RF ^{1}H–^{1}H decoupling is also applied during ^{1}H evolution. The exciting capabilities of directly and indirectly detected through-bond HETCOR NMR under fast MAS are illustrated on two naturally abundant solids, tripeptide *N-formyl*-L-methionyl-L-leucyl-L-phenylalanine (f-MLF-OH) and brown coal, one well ordered and the other highly disordered.

2. Background and experimental procedures

2.1. ^{1}H decoupling under fast MAS

Traditionally, high-resolution ^{1}H experiments were performed by combining rotation and multiple-pulse sequences (CRAMPS) operated under the quasi-static condition $\tau_c << \tau_R$, where $\tau_c = (\nu_c)^{-1}$ describes the cycle time of the pulse sequence which should be short compared to $\tau_R = (\nu_R)^{-1}$, and it is assumed that ν_c exceeds the strength of the homogeneous broadening to be removed [15,16]. The development of high-field magnets and probes capable of MAS at rates of up to 25 kHz (now regarded as moderate) was followed by the implementation of modified CRAMPS strategies, as thoroughly reviewed by Vega et al. [17]. Several decoupling techniques held promise for successful performance at even higher MAS speeds. These included PMLG and DUMBO [18], which can be used both in windowless and windowed schemes without rotor synchronization. The recently introduced symmetry-based rotor-synchronized sequences CN^{ν}_n, RN^{ν}_n and ZN^{ν}_n are also unrestricted by quasi-static approximation [12,19,20].

The PMLG sequence [21], which can be viewed as an on-resonance variant of the frequency-switched Lee–Goldburg (FSLG) experiment [22], suppresses the zero- and first-order terms in the average dipolar Hamiltonian. The basic version consists of two building blocks, each composed of a series of n pulses with sequentially advanced phases. It has been denoted as PMLGn^{Φ}_R [23], where Φ is the initial phase of the first block and R specifies the direction of phase rotation in the xy plane, with R = m for clockwise and R = p for counter clockwise rotation. This sequence proved easy to implement and yielded good resolution for n = 3, 5, and 9, although line broadening and RF-rotor frequency lines appeared at certain combinations of ν_c, ν_R and frequency offset values [24,25]. Windowed PMLG sequences (*w*PMLG) soon followed, providing opportunities for measuring 2D ^{1}H–^{1}H and indirectly detected ^{1}H{^{13}C} spectra [26]. The theoretical analysis of RF pulse imperfections led to the idea of using RF irradiation parameters (RF power and frequency offset) to obtain a *w*PMLGn^{Φ}_R sequence with an effective field along the z direction. This so called z-rotation yielded spectra with improved resolution and fewer artifacts [27,28]. Subsequently, the supercycled sequence PMLGn^{Φ}_R was introduced with $\Phi = \bar{\phi}\phi$ and R = mm, i.e., composed of two blocks PMLG$n^{\bar{\phi}}_m$ and PMLGn^{ϕ}_m, which relaxed the offset dependencies of the line-narrowing efficiency and the z-rotation (and thus the scaling factor which, however, is considerably reduced in the supercycled experiment) [23]. In all of these studies the condition $\nu_c > \nu_R$ was assumed and deemed necessary to achieve high resolution, provided that the periodicities associated with RF irradiation and MAS did not interfere; i.e., the condition $a\nu_R + b\nu_c = 0$ with a and b being small integers, was to be avoided. Most recently, however, it has been demonstrated that *w*PMLG5$^{\bar{x}\bar{x}}_{mm}$ (as well as *w*DUMBO) can perform comparably or better when applied at the highest available ν_R frequencies (up to 65 kHz), even under the condition $\nu_c < \nu_R$, as long as $|a/b|$ ratios are not equal to 1/2, 2/3, 1/3, etc. [11].

The family of rotor-synchronized SAM pulse sequences was recently introduced to achieve efficient homonuclear ^{1}H decoupling under very fast MAS by using smooth cosine modulation of the RF magnetic field amplitude [12]. We chose the SAM3 version of the sequence, with the modulation frequency $\nu_c = 3\nu_R$, because it does not reintroduce the heteronuclear dipolar and CSA interactions. It proved easy to optimize and tolerant of RF inhomogeneity, which made it potentially useful for our application.

Here, we tested the utility of PMLG and SAM3 decoupling during the INEPT transfer, although DUMBO and symmetry-based methods can be applied, as well. We were primarily concerned with slowing down the decoherence of the transverse magnetizations (T'_2 relaxation) of ^{1}H and ^{13}C nuclei during INEPT and less so with the minimization of artifacts such as zero peak, image peaks and RF-rotor frequency lines. Note, however, that the efficacy of these sequences in our experiments depends not only on their ability to slow down the T'_2 relaxation, but also on the scaling factors, which determine the effective J-coupling and the optimum duration of the polarization transfer.

2.2. Pulse sequences and optimization of homonuclear decoupling

The polarization transfer through chemical bond used here during mixing is based on a refocused INEPT (INEPTR) pulse sequence, which employs two pairs of rotor-synchronized delays. First, the antiphase proton magnetization is created during time delay $2\tau_1 \cong (2J_{CH})^{-1}$. A second pair of delays of similar duration τ_2 is used to refocus this magnetization into an in-phase signal. Note that the relaxation losses during INEPT are attributable to the polarizing nuclei during τ_1 and to those being polarized during τ_2. The transverse relaxation during τ_1 and τ_2 is mainly due to ^{1}H–^{1}H dipolar interaction, which we strive to overcome by using the combination of fast MAS and multiple-pulse sequences. The decoupling efficiency during INEPT can be conveniently assessed by measuring the ^{1}H (or ^{13}C) signal intensity versus τ in a simple spin-echo experiment shown in Fig. 1a, using the SAM3, PMLG5$^{\bar{x}}_m$ and PMLG5$^{\bar{x}\bar{x}}_{mm}$ decoupling sequences depicted in Fig. 1d. The ^{1}H measurements utilized direct polarization whereas ^{13}C data were measured following the ^{13}C{^{1}H} CP. The resulting spectra were used to evaluate the T'^{H}_2 and T'^{C}_2 relaxation times for all resolved proton and carbon sites in the f-MLF-OH tripeptide studied in this work.

The pulse sequence for the 2D HETCOR experiment with indirect detection of ^{13}C is shown in Fig. 1b. This sequence uses tangent ^{13}C{^{1}H} CP transfer, followed by t_1 evolution of ^{13}C magnetization, which is then stored along the B_0 field and transferred back to ^{1}H nuclei via INEPT [14]. The t_1-noise was minimized using the duty compensation of the RF power and by purging the ^{1}H magnetization during the $2\tau_{RR}$ period, as described earlier [8,29,30]. Fig. 1c depicts the corresponding ^{13}C-detected HETCOR scheme, which follows that proposed by Emsley et al. [13], but is operated here at high MAS rate [11]. Based on the analysis of relaxation data, only the PMLG5$^{\bar{x}}_m$ scheme was used during INEPTR in 2D experiments (i.e., during τ_1 and τ_2 in Fig. 1b and c). Both PMLG5$^{\bar{x}}_m$ and PMLG5$^{\bar{x}\bar{x}}_{mm}$ sequences were tested during the t_1 evolution of the ^{13}C-detected 2D experiment (Fig. 1c). SPINAL-64 heteronuclear decoupling is used during t_1 and t_2 periods, as appropriate [31]. In experiments performed under fast MAS ($\nu_R \geqslant 41.666$ kHz), a low RF magnetic field of $\sim\nu_R/4$ ($\sim$11 kHz in our experiments) was used during heteronuclear decoupling because it was as effective as a high RF magnetic field of $\sim$100 kHz at ν_R = 20.833 kHz [4,5,32].

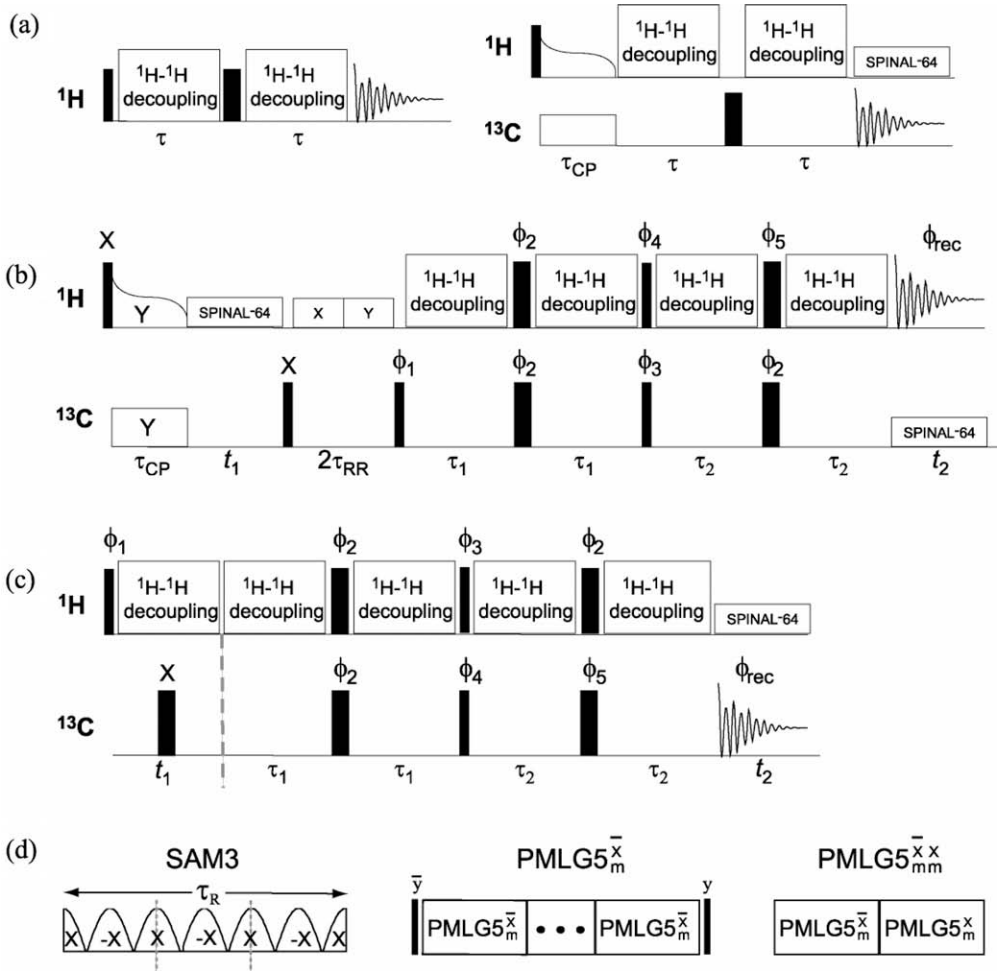

Fig. 1. Pulse sequences for ^{1}H and ^{13}C spin-echo (a), ^{1}H-detected through-bond HETCOR (b), and ^{13}C-detected through-bond HETCOR (c) experiments under fast MAS. Also shown are three RF ^{1}H homonuclear decoupling schemes (SAM3, PMLG5$^{\bar{x}}_{m}$ and PMLG5$^{\bar{x}x}_{mm}$) tested in these experiments (d). Note that in experiments involving PMLG5$^{\bar{x}}_{m}$ additional pulses were used before and after each decoupling pulse block to rotate ^{1}H magnetization from and into the *xy* plane. The effective field produced by the PMLG5$^{\bar{x}x}_{mm}$ sequence is almost parallel to the *z* axis, which leads to a broad-banded *z*-rotation of the magnetization and eliminates the need for preparatory pulses [23]. Solid rectangles represent $\pi/2$ and π pulses. The following phases were used in experiments (b) and (c): $\phi_1 = \{8x, 8(-x)\}$, $\phi_2 = 8\{x, -x\}$, $\phi_3 = 4\{y, y, -y, -y\}$, $\phi_4 = \{4x, 4y, 4(-x), 4(-y)\}$, $\phi_5 = 2\{x, -x, x, -x, y, -y, y, -y\}$, $\phi_{rec} = 2\{x, x, -x, -x, y, y, -y, -y\}$. States-TPPI detection was implemented in 2D experiments through appropriate phase switching of the first $\pi/2$ pulse in the ^{13}C channel. The SAM3 and PMLG sequences followed the recipes given in [12] and [23], respectively.

All experiments were carried out at 14.1 T on a Varian NMR System 600 spectrometer, using a FastMAS^{TM} probe operated at $\nu_R = 41.666$ kHz and 20.833 kHz. Additional experimental parameters are given in figure captions and table footnotes, using the following symbols: ν^X_{RF} denotes the magnitude of the RF magnetic field applied to X spins, τ_{CP} the CP time, τ_{RD} the recycle delay, τ_{RR} the rotary resonance recoupling time, Δt_1 the increment of t_1 during 2D acquisition, NS the number of scans, and AT the total acquisition time of a 2D spectrum. The ^{1}H and ^{13}C chemical shifts are reported using the δ scale and are referenced to TMS at 0 ppm.

The introduction of homonuclear decoupling schemes into the 2D sequences in Fig. 1 makes them appear complex to set up and optimize. However, we were able to maximize the performance of these sequences very simply by minimizing the signal loss due to T'^H_2 transverse relaxation in the spin-echo experiment shown in Fig. 1a. The experimental procedure involves the use of a single delay τ, and within a few minutes reliably provides the best choices for the pulse length, the RF power level, and the frequency offset. Because of the general relevance of this optimization to high-resolution ^{1}H spectroscopy, we will detail it separately in a forthcoming publication.

2.3. Samples

A common peptide and brown coal were chosen to demonstrate the applications of through-bond correlation methods. The solvent-free, naturally abundant tripeptide f-MLF-OH was purchased from Sigma–Aldrich. The f-MLF-OH structure features well resolved CH, CH_2, CH_3 and quaternary carbon sites, which exhibit a full range of ^{13}C–^{1}H couplings, from motionally narrowed to those typical of a fully rigid crystal lattice. The brown coal, originating from the former Cospuden coal mine near Leipzig (Germany), is chemically heterogeneous, which precludes the observation of sharp resonances in ^{1}H and ^{13}C NMR. Each sample was loaded into the MAS rotor under ambient conditions and studied at room temperature without any treatment.

3. Results and discussion

3.1. T'_2 relaxation

The T'^H_2 and T'^C_2 relaxation times were measured for f-MLF-OH using the spin-echo sequences shown in Fig. 1a. The data obtained

under MAS (ν_R = 41.667 kHz) and MAS with homonuclear decoupling (SAM3, PMLG5$^{\bar{x}}_{m}$ or PMLG5$^{\bar{x}\bar{x}}_{mm}$) are shown in Tables 1 and 2. Also shown are the relaxation data measured under PMLG5$^{\bar{x}}_{m}$ and PMLG5$^{\bar{x}\bar{x}}_{mm}$ decoupling with slower MAS (ν_R = 20.833 kHz). The relaxation times for individual sites were evaluated after acquiring spectra for 20 rotor-synchronized values of τ, as explained in the footnotes to the tables. Most of the carbon sites in f-MLF-OH could be easily resolved and assigned following an earlier report of Griffin et al. [33] (Fig. 2). The site-specific $T_2'^{C}$ values were not measured for F$^{\gamma}$ and carbonyl carbons (L′, F′ and M′) because they were of no interest to us, or for the pairs of carbons in the phenyl ring (F$^{\delta 1,2}$ and F$^{\varepsilon 1,2}$) because they remained broad and unresolved due to the interference of the ring dynamics (see below) with heteronuclear decoupling. In the case of $T_2'^{H}$ measurements, the RF homonuclear decoupling was not applied during ^{1}H detection, making resolution insufficient to resolve all proton sites (at ν_R = 41.667 kHz the resolution was comparable to that in Fig. 3b). Therefore, the ^{1}H spectra were deconvoluted into four groups of resonances centered at 0.8 ppm (representing CH_3 groups), 2.0 ppm (predominantly CH_2), 6.2 ppm (CH) and 8.8 ppm (formyl H), for which only the average values of $T_2'^{H}$ were evaluated by fitting the data with a single exponential decay. The performance of ^{1}H decoupling sequences was optimized as described in Section 2.2. Notably, under the PMLG sequences the best $T_2'^{H}$ and $T_2'^{C}$ values were obtained when ν_R was smaller than ν_c (e.g. in the case of PMLG5$^{\bar{x}\bar{x}}_{mm}$, $\nu_R/\nu_c \approx 0.62$ for ν_R = 41.667 kHz and $\nu_R/\nu_c \approx 0.56$ for ν_R = 20.833 kHz; see footnote (a) to Tables 1 and 2). Although similar $T_2'^{H}$ and $T_2'^{C}$ results could be reached under the condition $\nu_R > \nu_c$ (by adjusting the RF power level such that the two frequencies did not interfere), the resulting scaling factors were considerably reduced.

To facilitate the ensuing discussion, we note that in our measurements the ^{1}H and ^{13}C relaxation is influenced mainly by the residual homogeneous interactions that are non-refocusable by the rotor-synchronized π pulses under fast MAS and RF ^{1}H homonuclear decoupling. The refocusable (inhomogeneous) interactions include chemical shift anisotropy (CSA) and heteronuclear couplings. The ^{1}H and ^{13}C linewidths can be additionally broadened due to disorder and/or anisotropic bulk magnetic susceptibility [34–36]. Notwithstanding the simplicity of the spin-echo sequence, the measured relaxation times are difficult to rationalize because of the complexity of the spin dynamics in extended networks involving strongly interacting ^{1}H nuclei under MAS and RF decoupling, where the effective couplings depend on the orientation of the local networks with respect to the magnetic field. Numerical *ab initio* simulations reported recently by Zorin et al. [37] allowed for comprehensive analysis of ^{1}H linewidths in model systems with different dimensionalities and dynamics as a function of ν_R, in the absence of RF decoupling. In agreement with earlier predictions and measurements [38,39], the intrinsic homogeneous component of ^{1}H linewidth, as measured in the spin-echo experiment under MAS, was found to scale as $(\nu_R)^{-1}$, with the proportionality factor depending on the networks' dimensionality, geometry and dynamics [37]. The limit of homogeneous (spin-echo) linewidth at infinite ν_R is very low, because it is set by scalar J_{HH} couplings (which are typically on the order of 10 Hz and are invariant during this experiment) and the spin-spin relaxation T_2. Even when using MAS at the highest currently available rates, the potential exists to increase the efficiency of homonuclear decoupling with RF pulse sequences. By making the heteronuclear dipolar interaction with the dilute (^{13}C) nuclei inhomogeneous, efficient homonuclear decoupling has a similar effect on $T_2'^{C}$ processes.

Our measurements performed on organic-inorganic hybrid materials [14] and f-MLF-OH (data not included) also showed proportionality between $T_2'^{H}$ (as well as $T_2'^{C}$) and ν_R in the range of 20–42 kHz. In hybrid materials, the dipolar couplings in silica-bound species behaved inhomogeneously at ν_R = 40 kHz, yielding $T_2'^{H}$ and $T_2'^{C}$ relaxation times of more than 5 ms without the assistance of RF multiple-pulse sequences [14]. However, fast MAS alone proved insufficient in the case of a strongly coupled three-dimensional network of protons such as f-MLF-OH, where we observed sub-millisecond decays for many of the sites under similar conditions. By adding the RF decoupling, the decay of transverse magnetization was slowed down dramatically, 5- to 20-fold compared to that in fast MAS (Tables 1 and 2). In general, the PMLG5$^{\bar{x}\bar{x}}_{mm}$ decoupling proved superior, while SAM3 performed less efficiently than both PMLG5$^{\bar{x}}_{m}$ and PMLG5$^{\bar{x}\bar{x}}_{mm}$ sequences.

Although the overall effect of decoupling is remarkable, the data in Tables 1 and 2 show considerable disparity between relaxation times measured for different sites. The measurements of ^{1}H relaxation are difficult to interpret because they do not represent individual sites and functionalities. Most of the $T_2'^{H}$ times measured with PMLG decoupling at ν_R = 20.833 kHz are longer than those at ν_R = 41.667 kHz, whereas the $T_2'^{C}$ data are similar for most sites. Note, however, that the scaling factors are reduced at ν_R = 20.833 kHz.

In order to rationalize the results of $T_2'^{C}$ measurements, we note that parts of f-MLF-OH exhibit intrinsic motions at room temperature that are fast on the NMR timescale. These include the rotation

Table 1
Measurements of transverse relaxation time $T_2'^{H}$ in f-MLF-OH under MAS at 41.667 kHz, and MAS at 41.667 or 20.833 kHz with homonuclear RF pulse decoupling.

Functional group		δ_{1H} [ppm]	$T_2'^{H}$ [ms][a]					
			MAS only	SAM3	PMLG5$^{\bar{x}}_{m}$ [b]		PMLG5$^{\bar{x}\bar{x}}_{mm}$ [b]	
			s_f = 1.0	s_f = 0.71	s_f = 0.71	*0.49*	s_f = 0.36	*0.29*
CH	M^{α}, L^{α}, F^{α}, F^{δ}, F^{ε}, F^{ζ}	6.2	0.6	2.4	3.5	*5.2*	5.1	*5.9*
	Formyl	8.8	1.1	5.7	6.2	*9.6*	12.1	*8.2*
CH_2[c]	M^{δ}, M^{γ}, M^{β}, L^{β}, L^{γ}, F^{β}	2.0	0.6	3.8	5.3		10.3	
CH_3	$L^{\delta 1}$, $L^{\delta 2}$	0.8	0.4	2.1	4.4	*11.4*[d]	11.0	*15.2*[d]

[a] Each measurement consisted of 20 data points, which were fitted with a single exponential decay. The following rotor-synchronized increments of τ were used: $\Delta\tau$ = 24 μs (MAS), $\Delta\tau$ = 120 μs (SAM3), and $\Delta\tau$ = 240 μs (PMLG5$^{\bar{x}}_{m}$ and PMLG5$^{\bar{x}\bar{x}}_{mm}$). The data were acquired with τ_{RD} = 2 s using the RF magnetic fields ν^{H}_{RF} = 150 kHz during $\pi/2$, π and PMLG pulses, and ν^{H}_{RF} = 135 kHz during the SAM3 sequence. In the PMLG5$^{\bar{x}}_{m}$ experiment, additional short pulses (1.2 μs, ν^{H}_{RF} = 150 kHz) were used in the ^{1}H channel before and after each decoupling block to rotate ^{1}H magnetization from and into the *xy* plane. At ν_R = 41.667 kHz, the optimized homonuclear decoupling conditions were as follows: during SAM3, the cosine line shape was defined by 120 segments of 0.2 μs duration and total duration τ_c = 24 μs; during PMLG5$^{\bar{x}}_{m}$ and PMLG5$^{\bar{x}\bar{x}}_{mm}$ decoupling, we used τ_{PMLG} = 0.75 μs (τ_c = 7.5 and 15 μs, respectively). At ν_R = 20.833 kHz, only the PMLG5$^{\bar{x}}_{m}$ and PMLG5$^{\bar{x}\bar{x}}_{mm}$ decouplings were tested, which worked best with τ_{PMLG} = 1.35 μs (τ_c = 13.5 and 27 μs, respectively).

[b] Data obtained with ν_R = 20.833 kHz are given in italics.

[c] M^{δ} and L^{γ} are CH_3 and CH carbons, respectively.

[d] Resonances at 0.8 and 2.0 ppm were unresolved at ν_R = 20.833 kHz.

Table 2
Measurements of transverse relaxation time $T_2'^C$ in f-MLF-OH under MAS at 41.667 kHz, as well as MAS at 41.667 or 20.833 kHz with homonuclear RF pulse decoupling.

Functional group		δ_{13C} [ppm]	$T_2'^C$ [ms][a]					
			MAS only	SAM3	PMLG5$^{\bar{x}}_{m}$ [b]		PMLG5$^{\bar{x}x}_{mm}$ [b]	
			s_f = 1.0	s_f = 0.71	s_f = 0.71	*0.49*	s_f = 0.36	*0.29*
CH	M^{α}	52.0	2.2	11.7	26.8	*25.7*	26.9	*20.8*
	L^{α}	56.8	1.2	8.8	25.6	*22.3*	22.7	*18.8*
	L^{γ}	25.0	0.7	4.7	10.1	–[c]	5.4	–[c]
	F^{α}	54.3	1.4	9.7	17.5	*16.9*	18.5	*18.8*
	F^{ζ}	127.6	1.2	3.8	4.6	*7.7*	5.9	*6.4*
	Formyl	165.2	2.3	14.4	21.9	*17.4*	19.2	*12.6*
CH_2	M^{β}	37.5	0.9	4.9	7.6	*9.0*	9.6	*9.8*
	M^{γ}	28.7	0.9	4.0	5.1	*5.6*	7.1	*6.2*
	L^{β}	40.6	0.3	1.8	4.7	*5.4*	4.8	*5.9*
	F^{β}	36.9	0.7	2.0	3.9	*4.5*	5.0	*5.5*
CH_3	M^{δ}	14.0	5.3	9.1	11.4	*21.7*	25.1	*27.1*
	$L^{\delta 1}$	24.6	3.1	7.0	11.3	–[c]	18.2	–[c]
	$L^{\delta 2}$	19.6	2.7	6.6	10.6	*16.1*	19.1	*22.9*

[a] As in the case of $T_2'^H$ (Table 1), each measurement consisted of 20 data points, which were fitted with a single exponential decay. The following rotor-synchronized increments of τ were used: $\Delta\tau$ = 48 μs (MAS) and $\Delta\tau$ = 240 μs (SAM3, PMLG5$^{\bar{x}}_{m}$ and PMLG5$^{\bar{x}x}_{mm}$). At V_R = 41.667 KHz, the data were acquired with τ_{RD} = 2 s and τ_{CP} = 0.3 ms, using the RF magnetic fields ν^H_{RF} = 150 kHz during π/2 and PMLG pulses; ν^H_{RF} = 135 kHz during SAM3 sequence; ν^H_{RF} = 62 kHz during CP (tangent); ν^H_{RF} = 11 kHz during SPINAL-64 decoupling; ν^C_{RF} = 104 kHz during CP and π pulse. At V_R = 20.833 kHz, we used ν^H_{RF} = 52 kHz during CP (tangent), ν^H_{RF} = 100 kHz during SPINAL-64 decoupling and ν^C_{RF} = 74 kHz during CP. The optimized homonuclear decoupling conditions were the same as those described in Table 1 (footnote (a)).

[b] Data obtained with ν_R = 20.833 kHz are given in italics.

[c] At ν_R = 20.833 kHz, peaks at 25.0 and 24.6 ppm were not resolved because the acquisition period has been limited to 10 ms to lessen the burden of high-power decoupling on the NMR probe. Therefore, the $T_2'^C$ values could not be independently measured for L^{γ} and $L^{\delta 1}$.

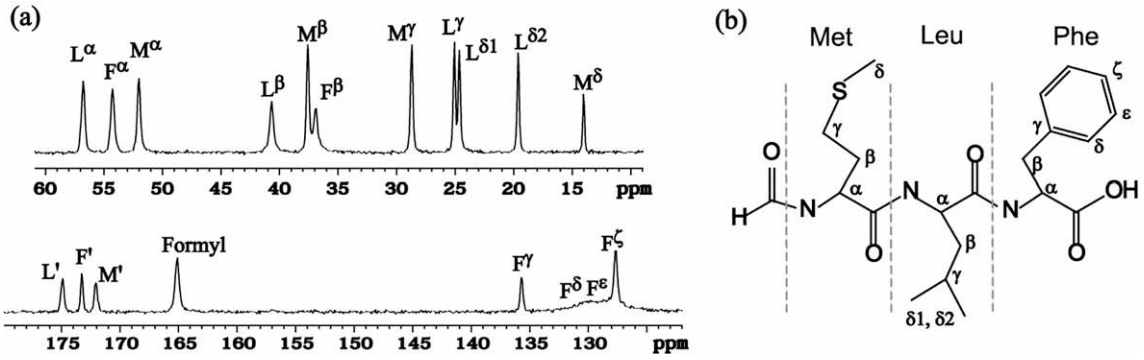

Fig. 2. ^{13}C CPMAS spectrum (a) and molecular structure of f-MLF-OH (b). The spectrum was measured at room temperature using ν_R = 41.667 kHz, τ_{CP} = 0.3 ms, ν^H_{RF} = 62 kHz during CP (tangent), ν^C_{RF} = 104 kHz during CP, ν^H_{RF} = 11 kHz during SPINAL-64 decoupling, and τ_{RD} = 2 s. The assignments are made following Refs. [33,40].

of methyl groups (carbons M^{δ}, $L^{\delta 1}$ and $L^{\delta 2}$) and 180° flips of the phenyl rings at a rate of $\sim 10^5$ s^{-1}; such rearrangements may be accommodated by additional motions of the surrounding chains. The ^1H–^{13}C couplings involving other carbons (M^{α}, L^{α}, L^{γ}, F^{α}, M^{β} and M^{γ}) were shown to be unaffected by motion at room temperature (see Ref. [40], Supporting Information). Accordingly, when both MAS and RF decoupling were used, the longest $T_2'^C$ times observed were for methyl (M^{δ}, $L^{\delta 1}$ and $L^{\delta 2}$) and CH (M^{α}, L^{α}, F^{α}) carbons. The methylene carbons (M^{β}, L^{β}, F^{β} and M^{γ}) relaxed faster, which suggests that further improvement can be achieved through more efficient decoupling. The L^{β} and F^{β} groups, however, also showed motional narrowing at room temperature [40], which may have interfered with decoupling. In the phenyl rings, carbons $F^{\delta 1,2}$ and $F^{\varepsilon 1,2}$ remained unresolved, whereas F^{ζ} also relaxed relatively fast, because the neighboring ^1H nuclei cannot be efficiently decoupled due to the flipping motion.

3.2. Efficiency of polarization transfer via INEPTR

Below we analyze the effect of RF decoupling on the efficiency of the INEPTR transfer in f-MLF-OH, focusing on fast MAS. The measurements of $T_2'^H$ and $T_2'^C$ showed that the PMLG5$^{\bar{x}}_{m}$ and PMLG5$^{\bar{x}x}_{mm}$ sequences performed better than SAM3. However, it is not immediately obvious which of the two PMLG schemes should be used, because of the effect of scaling factor s_f. The signal intensity observed in the INEPTR experiment can be written

$$\begin{aligned} I(\tau_1,\tau_2) &= \tfrac{\gamma_{exc}}{\gamma_{obs}} I_1(\tau_1) I_2(\tau_2) \\ &= \tfrac{\gamma_{exc}}{\gamma_{obs}} [\sin(2\pi J s_f \tau_1)] e^{-2\tau_1/T_2'^H} \\ &\quad [a_1 \sin(2\pi p_1 J s_f \tau_2) + a_2 \sin(2\pi p_2 J s_f \tau_2)] e^{-2\tau_2/T_2'^C} \end{aligned} \quad (1)$$

In ^{13}C-detected INEPTR the gyromagnetic ratios of the excited and observed nuclei are $\gamma_{exc} = \gamma_H$ and $\gamma_{obs} = \gamma_C$, respectively, and the precessions of the components of CH_n multiplets are given by

$$\begin{aligned} &CH: \quad a_1 = 1, p_1 = 1, a_2 = 0, \\ &CH_2: \quad a_1 = 1, p_1 = 2, a_2 = 0, \\ &CH_3: \quad a_1 = a_2 = \tfrac{3}{4}, p_1 = 1, p_2 = 3 \end{aligned} \quad (2)$$

We compared the effect of PMLG5$^{\bar{x}}_{m}$ and PMLG5$^{\bar{x}x}_{mm}$ on the evolutions of CH, CH_2 and CH_3 groups, using the average $T_2'^H$ and $T_2'^C$ values measured for each group, and assuming the same typical value

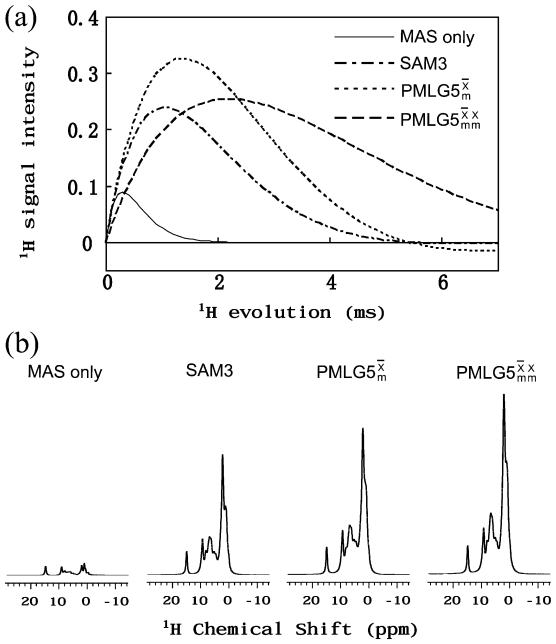

Fig. 3. (a) Decoherence of ^{1}H signal due to $T_2'^{H}$ as a function of τ measured for CH groups in f-MLF-OH under various decoupling conditions using the spin-echo sequence in Fig. 1a. The signal intensity is shown relative to that corresponding to infinitely long $T_2'^{H}$. (b) The corresponding ^{1}H spectra obtained at τ_1 = 1.2 ms.

of one-bond coupling J_{CH} = 130 Hz. The evolution during the polarization period (τ_1) for the CH groups in f-MLF-OH is shown in Fig. 3a, where the signal intensity expected under MAS and MAS with SAM3, PMLG5$^{\bar{x}}_{m}$ or PMLG5$^{\bar{x}x}_{mm}$ decoupling was calculated relative to that corresponding to infinitely long $T_2'^{H}$ (liquid-state, curve not shown). The effect of various decoupling schemes is further illustrated in Fig. 3b, which shows the ^{1}H intensities obtained using the spin-echo sequence in Fig. 1a with τ = 1.2 ms. The maximum intensities $I_1(\tau_1^{max})$ and $I_2(\tau_2^{max})$ expected in f-MLF-OH, as well as the corresponding delays τ_1^{max} and τ_2^{max}, are listed in Table 3. Also listed in the last column of Table 3 are the overall intensities $I_1(\tau_1)I_2(\tau_2)$.

Based on the results in Table 3, the PMLG5$^{\bar{x}}_{m}$ decoupling is most suitable for application during INEPTR, in spite of the fact that the PMLG5$^{\bar{x}x}_{mm}$ sequence yields longer $T_2'^{H}$ and $T_2'^{C}$ relaxation times. The use of PMLG5$^{\bar{x}}_{m}$ may reduce the relaxation losses by more than 10 times for CH and CH_2, and up to 7 times for CH_3 relative to fast MAS alone. Ultimately, one set of τ_1 and τ_2 values must be chosen in order to achieve the best overall sensitivity. In solution NMR this is achieved with $\tau_1 \cong 1/4J_{CH}$ and $\tau_2 \cong 0.3/J_{CH}$ (note that the requirement for full refocusing depends on multiplicity [41]), where J_{CH} is the typical expected value for the *J*-coupling: e.g., for J_{CH} = 130 Hz, τ_1 and τ_2 are both on the order of 2 ms. In samples with considerable range of couplings and multiplicities, non-ideal transfers are unavoidable. In solids, non-uniform T_2' relaxation may introduce additional inaccuracy. Still, our data suggest that by using τ_1 and τ_2 delays of around 1.5 ms, the overall efficiency of ^{1}H → ^{13}C INEPTR transfer should be on the order of 25% of the ideal transfer in liquid state. As noted in Section 3.1, for most sites the $T_2'^{H}$ and $T_2'^{C}$ times measured with PMLG decoupling at ν_R = 20.833 kHz are longer and similar, respectively, to those at ν_R = 41.667 kHz. However, this increase is more than offset by the reduced scaling factors (see Tables 1 and 2), leading to lower overall sensitivity.

The indirectly detected experiments utilizing ^{13}C → ^{1}H INEPTR should benefit from homonuclear ^{1}H decoupling in a similar way. In this case $\gamma_{exc} = \gamma_C$ and $\gamma_{obs} = \gamma_H$, yet the sensitivity ratio between solid-state and liquid-state experiments will remain similar to that given in the last column of Table 3.

Our 2D experiments, discussed in the sections below, have substantiated the above expectations.

3.3. 2D through-bond HETCOR spectra of f-MLF-OH

Here, the qualities of various approaches to 2D HETCOR NMR are assessed experimentally through a series of directly and indirectly detected measurements on tripeptide f-MLF-OH. The experimental schemes and conditions are summarized in Table 4, and selected spectra are shown in Figs. 4 and 5. All experiments were individually optimized and carried out under well-matched conditions. The ^{1}H-detected spectra used ^{1}H → ^{13}C cross-polarization to create initial ^{13}C magnetization, which imposed quantitative distortions consistent with those in Fig. 2a. Below we compare the overall sensitivity, resolution and structural information offered by these methods.

Sensitivity and resolution. Our experiments showed that high-quality through-bond HETCOR spectra can be obtained under fast MAS using both direct and indirect detection and confirmed that the sensitivity can indeed be dramatically increased by the use of homonuclear ^{1}H decoupling during τ_1 and τ_2 (Figs. 4 and 5).

In the top row of Fig. 5, the skyline ^{13}C projections of ^{1}H-detected spectra **5** and **6** (obtained without and with PMLG5$^{\bar{x}}_{m}$ decoupling during INEPTR) are shown along with the projections of ^{13}C-detected spectrum **1** (obtained with PMLG5$^{\bar{x}}_{m}$ decoupling applied only during INEPTR) and spectrum **2** (where PMLG5$^{\bar{x}}_{m}$ decoupling was also applied during t_1). Selected ^{1}H cross sections of peaks representing CH (M^{α}), CH_2 (M^{β}) and CH_3 ($L^{\delta 2}$) are compared below. In the case of ^{1}H{^{13}C} HETCOR, the S/N gain due to ^{1}H decoupling during INEPTR is approximately 10-fold for CH, at least 3-fold for CH_2 and 7-fold for CH_3 groups (compare Fig. 5a and b). For CH and CH_3 groups the result is approximately as expected from Table 3,

Table 3
The effect of decoupling during ^{1}H → ^{13}C INEPTR on the efficiency of polarization transfer in f-MLF-OH under fast MAS (ν_R = 41.667 kHz).

Group	RF decoupling	$T_2'^{H}$ [ms]	τ_1^{max} [ms]	$I_1(\tau_1^{max})$	$T_2'^{C}$ [ms][a]	τ_2^{max} [ms]	$I_2(\tau_2^{max})$	$I_1(\tau_1^{max})I_2(\tau_2^{max})$
CH	None	0.6	0.3	0.09	1.5	0.7	0.21	0.02
	PMLG5$^{\bar{x}}_{m}$	3.5	1.4	0.33	18	2.4	0.75	0.25
	PMLG5$^{\bar{x}x}_{mm}$	5.1	2.2	0.25	16	4.0	0.56	0.14
CH_2	None	0.6	0.3	0.09	0.9	0.4	0.25	0.02
	PMLG5$^{\bar{x}}_{m}$	5.3	1.7	0.44	5.3	1.1	0.64	0.28
	PMLG5$^{\bar{x}x}_{mm}$	10	3.3	0.43	6.6	1.9	0.50	0.21
CH_3	None	0.4	0.2	0.06	3.7	0.8	0.91	0.05
	PMLG5$^{\bar{x}}_{m}$	4.4	1.6	0.39	11	1.0	0.96	0.37
	PMLG5$^{\bar{x}x}_{mm}$	11	3.5	0.45	21	1.9	0.95	0.43

[a] These are average $T_2'^{C}$ values for each group calculated from the data in Table 2.

Table 4
The list of 2D HETCOR experiments performed on f-MLF-OH. The experiments used the pulse sequences shown in Fig. 1b and c, and were individually optimized as explained in Section 2.2.

Experiment[a]		ν_R [kHz]	Decoupling during t_1	Mixing	τ_1^{max} [ms]	τ_2^{max} [ms]	Decoupling during τ_1,τ_2	Decoupling during t_2
1	$^{13}C\{^1H\}$	41.667	SPINAL-64	INEPTR	1.20	0.84	$PMLG5^{\bar{x}}_{m}$	SPINAL-64
2	$^{13}C\{^1H\}$	41.667	$PMLG5^{\bar{x}}_{m}$	INEPTR	1.20	0.84	$PMLG5^{\bar{x}}_{m}$	SPINAL-64
3	$^{13}C\{^1H\}$	41.667	$PMLG5^{\bar{x}\bar{x}}_{mm}$	INEPTR	1.20	0.84	$PMLG5^{\bar{x}}_{m}$	SPINAL-64
4	$^{13}C\{^1H\}$	20.833	$PMLG5^{\bar{x}}_{m}$	INEPTR	1.68	1.44	$PMLG5^{\bar{x}}_{m}$	SPINAL-64
5	$^1H\{^{13}C\}$	41.667	SPINAL-64	INEPTR	0.31	0.22	–	SPINAL-64
6	$^1H\{^{13}C\}$	41.667	SPINAL-64	INEPTR	0.84	1.20	$PMLG5^{\bar{x}}_{m}$	SPINAL-64
7	$^1H\{^{13}C\}$	41.667	SPINAL-64	CP	–		–	SPINAL-64

[a] All measurements were performed with a fully loaded rotor (~8 μL). Initial ^{13}C polarization in the ^1H-detected experiments (**5**–**7**) was produced via CP under the conditions given in the caption to Fig. 2. The homo- and heteronuclear ^1H decoupling conditions were the same as given in footnote (a) to Tables 1 and 2. During the acquisition of ^1H-detected spectra, SPINAL-64 heteronuclear decoupling performed very well at low power (ν^C_{RF} = 11 kHz). Additional experimental details are as follows: experiment **1**: NS = 64, Δt_1 = 24 μs (64 rows), AT = 4.7 h; experiment **2**: NS = 16, Δt_1 = 15 μs (300 rows), AT = 5.5 h; experiment **3**: NS = 16, Δt_1 = 30 μs (300 rows), AT = 5.5 h; experiment **4**: NS = 16, Δt_1 = 27 μs (190 rows), AT = 3.5 h; experiment **5**: τ_{RR} = 48 ms, NS = 32, Δt_1 = 24 μs (800 rows), AT = 30 h; experiment **6**: τ_{RR} = 48 ms, NS = 16, Δt_1 = 24 μs (800 rows), AT = 15 h; and experiment **7**: τ_{RR} = 48 ms, τ_{CP} = 0.3 ms, NS = 16, Δt_1 = 24 μs (800 rows), AT = 15 h.

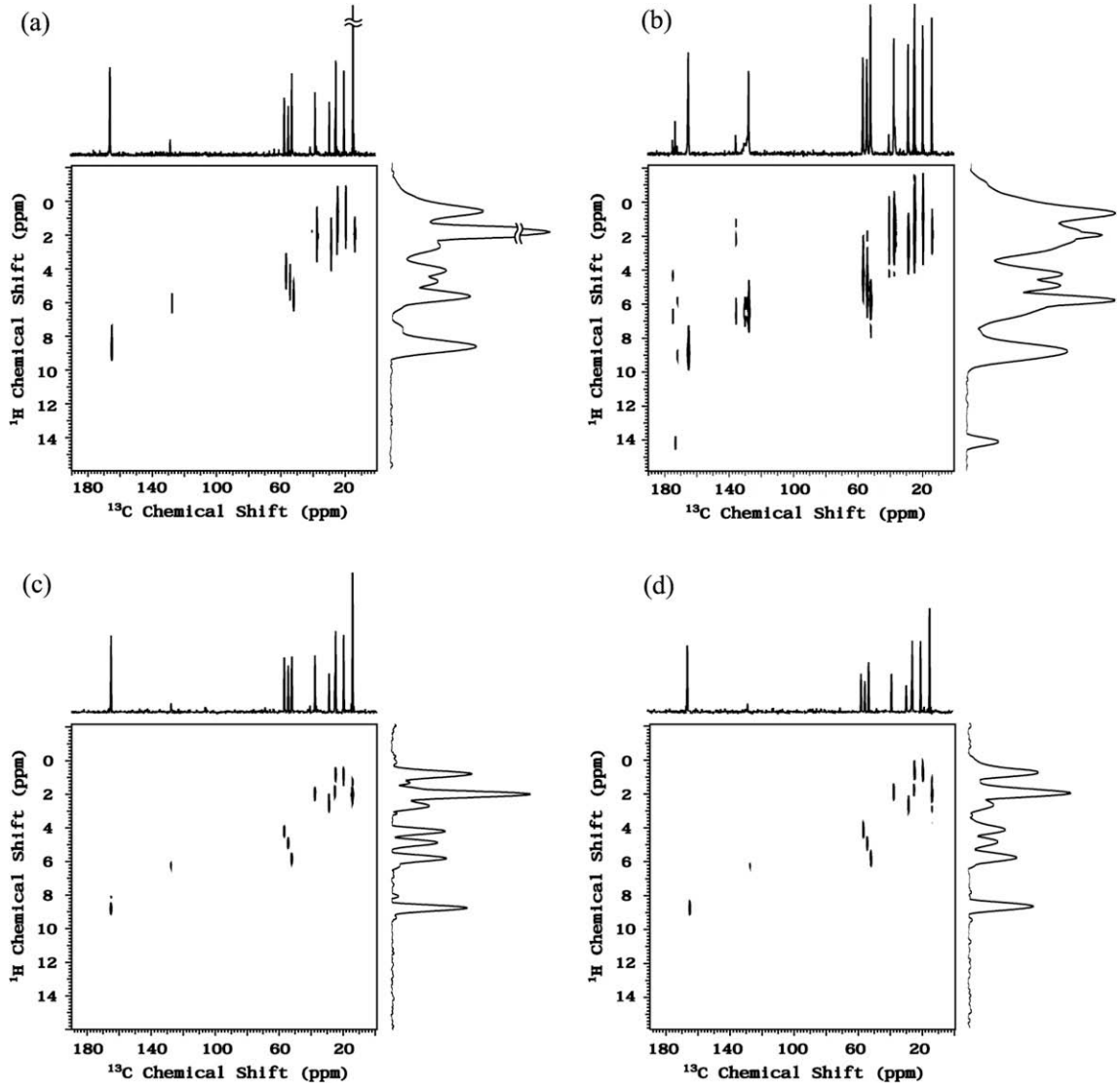

Fig. 4. 2D HETCOR spectra of f-MLF-OH obtained using (a) ^1H detection, INEPTR mixing and ν_R = 41.667 kHz, (b) ^1H detection, CP mixing and ν_R = 41.667 kHz, (c) ^{13}C detection, INEPTR mixing and ν_R = 41.667 kHz and (d) ^{13}C detection, INEPTR mixing and ν_R = 20.833 kHz (experiments **6**, **7**, **2** and **4**, respectively). Acquisition times were 15 h (a,b), 5.5 h (c) and 3.5 h (d). Other experimental details are given in the footnotes to Tables 1, 2 and 4. Note that the spectra acquired with ν_R = 41.667 kHz (a–c) used low-power SPINAL-64 decoupling. Since spectrum (d) required the use of high power (ν^H_{RF} = 100 kHz, see Table 2), the acquisition period was limited to 10 ms. To compare spectra (c) and (d), the former was also broadened accordingly. Such broadening was not applied to this spectrum in Fig. 5.

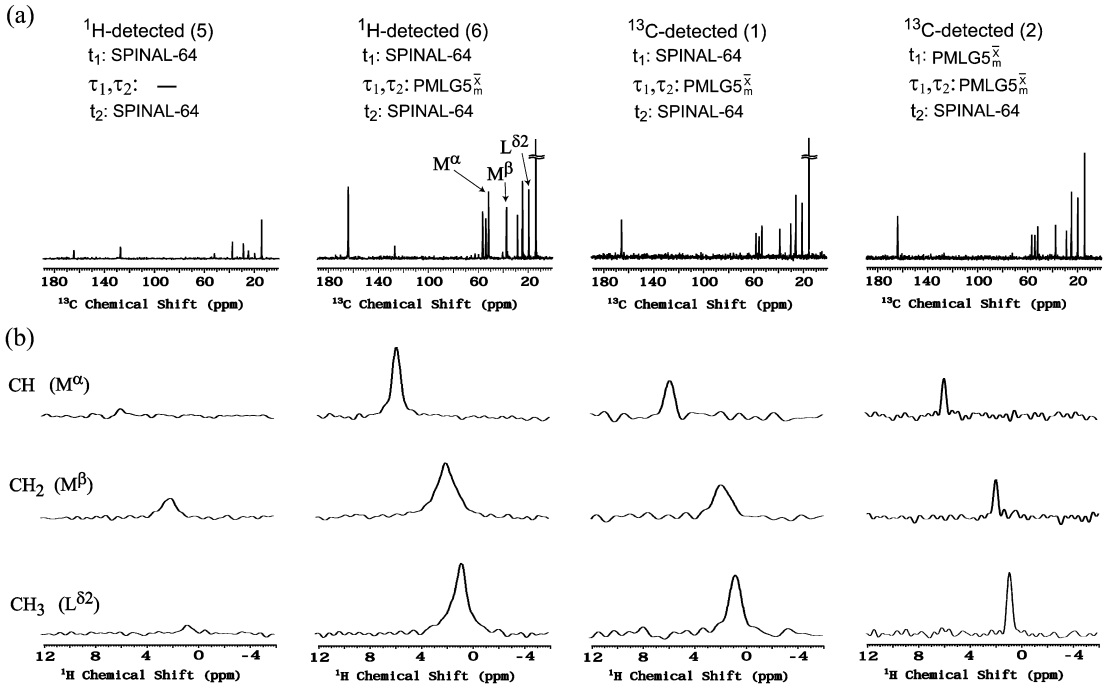

Fig. 5. (a) 1D ^{13}C skyline projections and (b) representative ^{1}H slices from spectra **5**, **6**, **1** and **2**. All experiments used mixing via INEPTR and MAS at 41.667 kHz. For clarity, the decoupling conditions are listed at the top of each column. Other experimental details are given in footnotes to Tables 1, 2 and 4. The spectra are normalized such that the peak heights are proportional to sensitivity per scan.

although the maximum intensity was observed at lower-than-expected values of τ_1 and τ_2 (compare Tables 3 and 4). It is clear in Fig. 4a, c, d and Fig. 5 that the methyl carbons and all carbons exhibiting strong (i.e. unaffected by motion) ^{1}H–^{13}C couplings (M$^\alpha$, L$^\alpha$, F$^\alpha$, M$^\beta$, M$^\gamma$, L$^\gamma$ and formyl groups) can achieve through-bond polarization relatively easily. The methylene carbons L$^\beta$ and F$^\beta$, resonating at 40.6 ppm and 36.9 ppm, are polarized less efficiently, as expected from the transverse relaxation data.

When comparing the indirect and direct methods we recall that the sensitivity gain not only depends on the polarization efficiency, but is also proportional to $(\gamma_{obs}/\gamma_{exc})^{3/2}$ and to the square root of the NMR linewidths in Hz $(\Delta\nu_{exc}/\Delta\nu_{obs})^{1/2}$ [6]. Remarkably, the ^{1}H-detected experiment **6** provided higher overall S/N per unit time than ^{13}C-detected experiments **1** and **2** (Fig. 5), in spite of the unfavourable linewidth ratio in f-MLF-OH. However, experiment **2** yielded much better resolution in the ^{1}H dimension, making it potentially advantageous in studies of complex molecules. In this context, it is important to note that the use of PMLG5$^{\bar{x}\bar{x}}_{mm}$ during t_1, which we tested in experiment **3** (spectrum not shown), did not offer any advantage yielding a spectrum with similar ^{1}H linewidths (in ppm) and sensitivity as that in experiment **2** (Fig. 4c).

Fast MAS versus 'slow' MAS. The merit of using fast MAS in ^{13}C-detected INEPT experiments can be gauged by comparing the best spectra taken at ν_R = 41.667 kHz and 20.883 kHz (experiments **2** and **4**, shown in Fig. 4c and d, respectively). Optimization of these experiments yielded different conditions for ^{1}H homonuclear decoupling, as shown in footnote (a) to Table 1. When experiment **4** was performed under the ^{1}H decoupling conditions optimal for experiment **2**, the spectrum lacked sensitivity, especially with regard to methylene groups, which were almost completely lost (spectrum not shown). We further note that in experiment **4** the SPINAL-64 ^{1}H decoupling had to be performed using a high RF magnetic field of $\nu^H_{RF} \cong 100$ kHz. To lessen the burden on the probe, the acquisition period t_2 was limited to 10 ms, causing broadening of the ^{13}C lines. In order to make spectra **2** and **4** easier to compare, spectrum **2**, which was acquired without truncation under low-power decoupling and is displayed in Fig. 4c, was broadened accordingly during processing. Although spectrum **2** has comparable S/N per unit time, it is better resolved in the ^{1}H dimension and more quantitative than the one obtained with ν_R = 20.883 kHz. Perhaps the resolution in spectrum **4** could be improved by reducing the sample volume to improve the homogeneity of the RF magnetic field.

Through-bond versus through-space correlations. Finally, it is instructive to compare the through-bond ^{1}H{^{13}C} correlation spectra with those obtained using CP under otherwise identical conditions (experiments **6** and **7**, spectra shown in Fig. 4a and b, respectively). To maximize the polarization of carbon sites, the CP-based spectrum was acquired using τ_{CP} of 0.3 ms. For protonated carbons, the sensitivity of this spectrum is 1.5-2 times higher than that of spectrum **6**. As expected, it features a number of additional correlations involving all carbons identified in the 1D CPMAS spectrum of f-MLF-OH (Fig. 2a). These long-range correlations can be suppressed by limiting the contact time to less than 50 μs, which would considerably reduce the overall sensitivity. Bearing in mind that CP-based can be affected by motion, RF homogeneity, and $T_{1\rho}$ relaxation, our results show that through-bond correlation NMR spectroscopy under fast MAS can be a very effective tool for studying fully coupled, naturally abundant solids.

3.4. 2D HETCOR spectra of brown coal

Fossil fuels are structurally very heterogeneous, which is reflected in their ^{1}H and ^{13}C solid-state NMR spectra. Even when state-of-the-art line narrowing methods are used, the solid-state NMR spectra of both nuclei feature relatively broad bands representing sp, sp^2 and sp^3 functionalities. The structual characterization of coals by NMR has been mainly confined to utilization of liquid-state studies of coal-derived liquids and 1D spectral editing techniques developed for simplification of solid-state spectra [42]. Until now, relatively few 2D solid-state NMR experiments have been applied to this purpose [42–44].

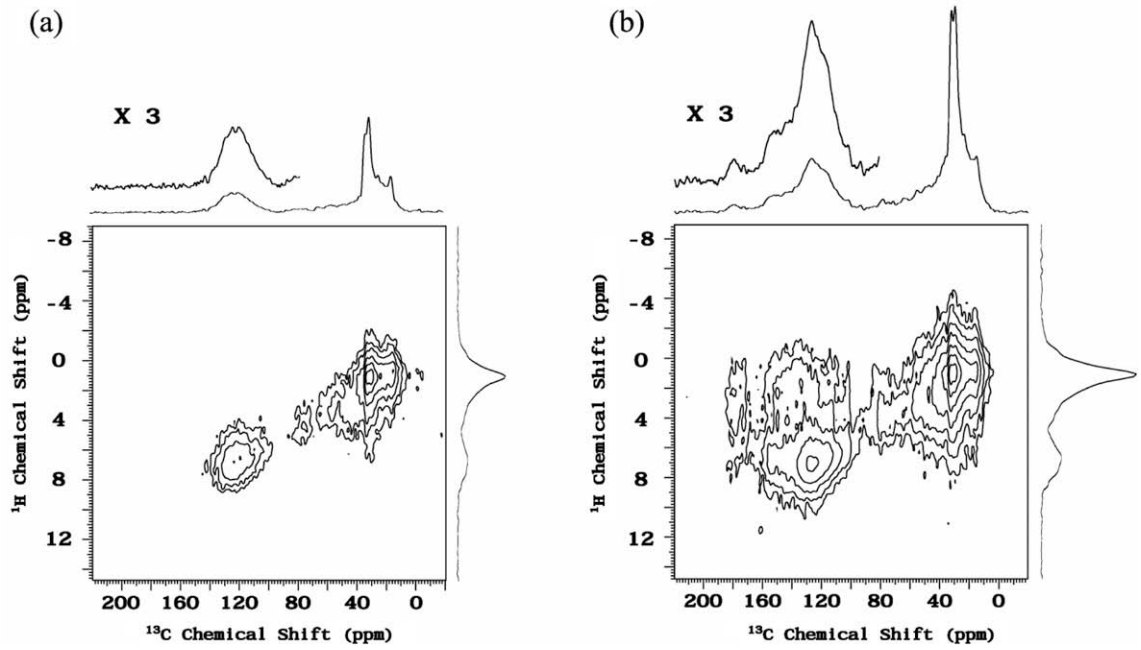

Fig. 6. 2D $^{1}H\{^{13}C\}$ HETCOR spectra of brown coal acquired using INEPTR (a) and CP (b) transfers during mixing. The following RF magnetic fields were used: ν_{RF}^{H} = 150 kHz during $\pi/2$ and PMLG5$_{m}^{\bar{x}}$ pulses, ν_{RF}^{H} = 62 kHz during CP (tangent), ν_{RF}^{H} = 11 kHz during SPINAL-64 decoupling in t_1, ν_{RF}^{C} = 104 kHz during CP, $\pi/2$ and π pulses, and ν_{RF}^{C} = 11 kHz during SPINAL-64 decoupling in t_2. Other experimental conditions were as follows: ν_R = 41.667 kHz, τ_{CP} = 1.5 ms, τ_{RR} = 24 ms, τ_1 = 0.84 ms, τ_2 = 1.2 ms, τ_{PMLG} = 0.75 μs, τ_c = 7.5 μs, τ_{RD} = 0.8 s, NS = 176, Δt_1 = 24 μs (100 rows), and AT = 8.7 h.

Indirectly detected $^{1}H\{^{13}C\}$ spectra of brown coal were acquired with mixing via INEPTR (experiment **6**, Fig. 6a) and CP (experiment **7**, Fig. 6b), yielding comparable intensities. Experiment **2** (^{13}C-detected, not shown) was also performed, but was less sensitive and did not provide improved resolution in the ^{1}H dimension. The INEPTR-based spectrum in Fig. 6a does not feature any ^{13}C resonances near 180 ppm, which are quite intense in the CP-based spectrum. This range of chemical shifts represents various types of carbonyl groups, in particular those involved in aldehyde and carboxylic functionalities. Another 'missing' resonance in Fig. 6a is one centred at 150 ppm, generally associated with various types of quaternary aromatic carbons, including aliphatic chain- and oxygen-bound carbons. A discernible resonance near 80 ppm is present in both spectra, which suggests the presence of sp carbons in alkynes and sp^2 carbons in olefins.

4. Conclusions

J-couplings can be successfully exploited in directly and indirectly detected 2D HSQC-type HETCOR experiments under fast MAS (∼42 kHz), providing through-bond ^{13}C–^{1}H correlations in naturally abundant solids with an efficiency that rivals that of traditional through-space experiments. Efficient ^{1}H decoupling plays a key role in preventing the decoherence of ^{1}H and ^{13}C magnetizations during polarization transfer via INEPTR. Among the tested decoupling schemes (PMLG5$_{m}^{\bar{x}}$, PMLG5$_{mm}^{\bar{x}\bar{x}}$ and SAM3), PMLG5$_{m}^{\bar{x}}$ proved most suitable, providing sensitivity gains of 3-10 in strongly coupled ^{1}H–^{13}C pairs. The best results were obtained when ν_R was smaller than ν_c (in the case of PMLG5$_{mm}^{\bar{x}\bar{x}}$ for $\nu_R/\nu_c \approx 0.62$) due to good decoupling efficiency and a high scaling factor. At ultrahigh speeds (∼70 kHz), the SAM3 method may become competitive with PMLG schemes.

2D HETCOR spectra of well ordered (crystalline tripeptide f-MLF-OH) and highly disordered (brown coal) samples were measured and analyzed. In spite of an unfavourable ^{1}H to ^{13}C linewidth ratio in f-MLF-OH, the indirect detection method offered higher overall sensitivity. However, in cases where ^{1}H resolution under fast MAS alone is unsatisfactory, ^{13}C detection with ^{1}H homonuclear decoupling during t_1 may be the method of choice. Our measurements showed that experiments performed under fast MAS compare favorably with those carried out at a lower spinning rate (∼21 kHz). Proper optimization of ^{1}H homonuclear decoupling proved very important in achieving high efficiency and resolution. A simple and reliable optimization scheme was used, which will be detailed in a forthcoming publication. The through-bond polarization transfer will undoubtedly become an important addition to cross-polarization in designing new multidimensional schemes dedicated for high-field, fast-MAS applications.

Acknowledgments

This research was supported at the Ames Laboratory by the US Department of Energy, Office of Basic Energy Sciences, under Contract No. DE-AC02-07CH11358. The authors thank Drs. S. Vega, J.-P. Amoureux and M. Hong for helpful discussions and Dr. J. Wiench for experimental assistance. The sample of brown coal was kindly provided by Prof. D. Michel.

References

[1] A. Samoson, Extended magic-angle spinning, in: D.M.R. Grant, K. Harris (Eds.), Encyclopedia of Nuclear Magnetic Resonance, vol. 9, John Wiley & Sons, Chichester, 2002, pp. 59–64.
[2] L.S. Du, A. Samoson, T. Tuherm, C.P. Grey, 19F/23Na double resonance MAS NMR study of oxygen/fluorine ordering in the oxyfluoride Na5W3O9F5, Chem. Mater. 12 (2000) 3611–3616.
[3] M. Ernst, A. Detken, A. Böckmann, B.H. Meier, NMR spectra of a microcrystalline protein at 30 kHz MAS, J. Am. Chem. Soc. 125 (2003) 15807–15810.
[4] J. Trebosc, J.W. Wiench, S. Huh, V.S.-Y. Lin, M. Pruski, Studies of organically functionalized mesoporous silicas using heteronuclear solid-state correlation NMR spectroscopy under fast magic angle spinning, J. Am. Chem. Soc. 127 (2005) 7587–7593.
[5] M. Ernst, M.A. Meier, T. Tuherm, A. Samoson, B.H. Meier, Low-power high-resolution solid-state NMR of peptides and proteins, J. Am. Chem. Soc. 126 (2004) 4764–4765.

[6] Y. Ishii, R. Tycko, Sensitivity enhancement in solid state 15N NMR by indirect detection with high-speed magic angle spinning, J. Magn. Reson. 142 (2000) 199–204.
[7] B. Reif, R.G. Griffin, ^{1}H detected ^{1}H, ^{15}N correlation spectroscopy in rotating solids, J. Magn. Reson. 160 (2003) 78–83.
[8] J.W. Wiench, C.E. Bronniman, V.S.-Y. Lin, M. Pruski, Chemical shift correlation NMR spectroscopy with indirect detection in fast rotating solids: studies of organically functionalized mesoporous silicas, J. Am. Chem. Soc. 129 (2007) 12076–12077.
[9] D.H. Zhou, G. Shah, M. Cormos, C. Mullen, D. Sandoz, C.M. Rienstra, Proton-detected solid-state NMR spectroscopy of fully protonated proteins at 40 kHz magic-angle-spinning, J. Am. Chem. Soc. 129 (2007) 11791–11801.
[10] D.H. Zhou, C.M. Rienstra, Rapid analysis of organic compounds by proton-detected heteronuclear correlation NMR spectroscopy with 40 kHz magic angle spinning, Angew. Chem. Int. Ed. 47 (2008) 7328–7331.
[11] M. Leskes, S. Steuernagel, D. Schneider, P.K. Madhu, S. Vega, Homonuclear dipolar decoupling at magic angle spinning frequencies up to 65 kHz in solid-state nuclear magnetic resonance, Chem. Phys. Lett. 466 (2008) 95–99.
[12] J.-P. Amoureux, B. Hu, J. Trebosc, Enhanced resolution in proton solid-state NMR with very fast MAS experiments, J. Magn. Reson. 193 (2008) 305–307.
[13] B. Elena, A. Lesage, S. Steuernagel, A. Böckmann, L. Emsley, Proton to carbon-13 INEPT in solid-state NMR spectroscopy, J. Am. Chem. Soc. 127 (2005) 17296–17302.
[14] K. Mao, J.W. Wiench, V.S.-Y. Lin, M. Pruski, Indirectly detected through-bond chemical shift correlation NMR spectroscopy under fast MAS: studies of organic–inorganic hybrid materials, J. Magn. Reson. 196 (2009) 92–95.
[15] M. Mehring, J.S. Waugh, Magic-angle NMR in solids, Phys. Rev. B 5 (1972) 3459–3481.
[16] B.C. Gerstein, R.G. Pembleton, R.C. Wilson, L.M.J. Ryan, High resolution NMR in randomly oriented solids with homonuclear dipolar broadening: combined multiple pulse NMR and magic angle spinning, Chem. Phys. 66 (1977) 361–362.
[17] E. Vinogradov, P.K. Madhu, S. Vega, Strategies for high-resolution proton spectroscopy, Top. Curr. Chem. 246 (2004) 33–90.
[18] D. Sakellariou, A. Leasge, P. Hodgkinson, L. Emsley, Homonuclear dipolar decoupling in solid-state NMR using continuous phase modulation, Chem. Phys. Lett. 319 (2000) 253–260.
[19] P.K. Madhu, X. Zhao, M.H. Levitt, High-resolution ^{1}H NMR in the solid state using symmetry-based pulse sequences, Chem. Phys. Lett. 346 (2001) 142–148.
[20] S. Paul, R.S. Thakur, P.K. Madhu, ^{1}H homonuclear dipolar decoupling at high magic-angle spinning frequencies with rotor-synchronized symmetry sequences, Chem. Phys. Lett. 456 (2008) 253–256.
[21] E. Vinogradov, P.K. Madhu, S. Vega, High-resolution proton solid-state NMR spectroscopy by phase-modulated Lee–Goldburg experiment, Chem. Phys. Lett. 314 (1999) 443–450.
[22] A. Bielecki, A.C. Kolbert, M.H. Levitt, Frequency-switched pulse sequences – homonuclear decoupling and dilute spin NMR in solids, Chem. Phys. Lett. 155 (1989) 341–346.
[23] M. Leskes, P.K. Madhu, S. Vega, A broad-banded z-rotation windowed phase-modulated Lee–Goldburg pulse sequence for ^{1}H spectroscopy in solid-state NMR, Chem. Phys. Lett. 447 (2007) 370–374.
[24] E. Vinogradov, P.K. Madhu, S. Vega, A bimodal Floquet analysis of phase modulated Lee–Goldburg high resolution proton magic angle spinning NMR experiments, Chem. Phys. Lett. 329 (2000) 207–214.
[25] E. Vinogradov, P.K. Madhu, S. Vega, Phase-modulated Lee–Goldburg magic angle spinning proton nuclear magnetic resonance experiments in the solid state: a bimodal Floquet theoretical treatment, J. Chem. Phys. 115 (2001) 8983–9000.
[26] E. Vinogradov, P.K. Madhu, S. Vega, Proton spectroscopy in solid-state nuclear magnetic resonance with windowed phase modulated Lee–Goldburg decoupling sequences, Chem. Phys. Lett. 354 (2002) 193–202.
[27] L. Bosman, P.K. Madhu, S. Vega, E. Vinogradov, Improvement of dipolar decoupling sequences in solid-state nuclear magnetic resonance utilizing radiofrequency imperfections, J. Magn. Reson. 169 (2004) 39–48.
[28] M. Leskes, P.K. Madhu, S. Vega, Proton line narrowing in solid-state nuclear magnetic resonance: new insights from windowed phase-modulated Lee–Goldburg sequence, J. Chem. Phys. 125 (2006) 124506. 1–18.
[29] E.K. Paulson, C.R. Morcombe, V. Gaponenko, B. Dancheck, R.A. Byrd, K.W. Zilm, Sensitive high resolution inverse detection NMR spectroscopy of proteins in the solid state, J. Am. Chem. Soc. 125 (2003) 15831–15836.
[30] Y. Ishii, J.P. Yesionowski, R. Tycko, Sensitivity enhancement in solid-state ^{13}C NMR of synthetic polymers and biopolymers by ^{1}H NMR detection with high-speed magic angle spinning, J. Am. Chem. Soc. 123 (2001) 2921–2922.
[31] B.M. Fung, A.K. Khitrin, K. Ermolaev, An improved broadband decoupling sequence for liquid crystals and solids, J. Magn. Reson. 142 (2000) 97–101.
[32] M. Ernst, A. Samoson, B.H. Meier, Low-power decoupling in fast magic-angle spinning NMR, Chem. Phys. Lett. 348 (2001) 293–302.
[33] C.M. Rienstra, L. Tucker-Kellogg, C.P. Jaroniec, M. Hohwy, B. Rief, M.T. McMahon, B. Tidor, T. Lozano-Perez, R.G. Griffin, De novo determination of peptide structure with solid-state magic-angle spinning NMR spectroscopy, Proc. Natl. Acad. Sci. USA 99 (2002) 10260–10265.
[34] A.N. Garroway, D.L. VanderHart, W.L. Earl, ^{13}C n.m.r. in organic solids: limits to spectral resolution and to determination of molecular motion, Philos. Trans. R. Soc. London A 299 (1981) 609–641.
[35] U. Schwerk, D. Michel, M. Pruski, Local magnetic field distribution in a polycrystalline sample exposed to a strong magnetic field, J. Magn. Reson. 119A (1996) 157–164.
[36] A. Samoson, T. Tuherm, Z. Gan, High-field high-speed MAS resolution enhancement in ^{1}H NMR spectroscopy of solids, Solid State Nucl. Magn. Reson. 20 (2001) 130–136.
[37] V.E. Zorin, S.P. Brown, P. Hodgkinson, Origins of linewidth in ^{1}H magic-angle spinning NMR, J. Chem. Phys. 125 (2006) 144508.
[38] E. Brunner, D. Freude, B.C. Gerstein, H. Pfeifer, Residual linewidths of NMR-spectra of spin-1/2 systems under magic-angle spinning, J. Magn. Reson. 90 (1990) 90–99.
[39] U. Haeberlen, J.S. Waugh, Coherent averaging effects in magnetic resonance, Phys. Rev. 175 (1968) 453–467.
[40] V.S. Bajaj, P.C.A. van der Wel, R.G. Griffin, Observation of a low-temperature, dynamically driven structural transition in a polypeptide by solid-state NMR spectroscopy, J. Am. Chem. Soc. 131 (2009) 118–128.
[41] D.T. Pegg, D.M. Doddrell, W.M. Brooks, M.R. Bendall, Proton polarization transfer enhancement for a nucleus with arbitrary spin quantum number from *n*-scalar coupled protons for arbitrary preparation times, J. Magn. Reson. 44 (1981) 32–40.
[42] R.E. Botto, Fossil fuels, in: D.M. Grant, R.K. Harris (Eds.), Encyclopedia of Nuclear Magnetic Resonance, vol. 3, John Wiley & Sons, Chichester, 1996, pp. 2101–2118.
[43] K.W. Zilm, G.G. Webb, C-13 proton shift correlation spectroscopy of a whole coal, Fuel 65 (1986) 721–724.
[44] J.Z. Hu, M.S. Solum, C.M.V. Taylor, R.J. Pugmire, D.M. Grant, Structural determination in carbonaceous solids using advanced solid-state NMR techniques, Energy Fuels 15 (2001) 14–22.